Synthesis, Characterization and Electrochemical Properties of Optically Active [60]Fullerene Organotransition Metal Complexes *mer*-[(η^2-C_{60})M(CO)$_3${(−)-DIOP}] (M = Mo, W), *mer*-[(η^2-C_{60})M(CO)$_3${(+)-DIOP}] (M = Mo, W) and [(η^2-C_{60})M{(−)-DIOP}] (M = Pd, Pt) − Crystal Structure of [(η^2-C_{60})Pt{(−)-DIOP}]

Li-Cheng Song,*[a] Peng-Chong Liu,[a] Jin-Ting Liu,[a] Fu-Hai Su,[a] Guang-Feng Wang,[a] Qing-Mei Hu,[a] Piero Zanello,[b] Franco Laschi,[b] and Marco Fontani[b]

Keywords: Transition metals / Fullerenes / Electrochemistry / Optical activity

This paper reports on several new optically active organometallic [60]fullerene complexes that contain a chiral (+)-DIOP or (–)-DIOP ligand [DIOP = 2,3-*O*,*O*′-isopropylidene-2,3-dihydroxy-1,4-bis(diphenylphosphanyl)butane]. The Mo/W complexes *mer*-[(η^2-C_{60})M(CO)$_3${(–)-DIOP}] (**1**, M = Mo; **2**, M = W) and *mer*-[(η^2-C_{60})M(CO)$_3${(+)-DIOP}] (**3**, M = Mo; **4**, M = W) were synthesized by a photochemical reaction of a mixture of [M(CO)$_6$], (–)-DIOP or (+)-DIOP and C_{60} in chlorobenzene in 42–51% yields, whereas the Pd/Pt complexes [(η^2-C_{60})M{(–)-DIOP}] (**5**, M = Pd; **6**, M = Pt) were prepared by a thermal reaction of C_{60} with [M(PPh$_3$)$_4$], followed by in situ treatment of the intermediate [(η^2-C_{60})M(PPh$_3$)$_2$] with (–)-DIOP, in toluene in > 90% yields. All the new complexes **1**–**6** were fully characterized by elemental analysis, ^{1}H (^{31}P, ^{13}C) NMR, IR, UV/Vis and circular dichroism (CD) spectroscopy. The structure of [(η^2-C_{60})Pt{(–)-DIOP}] (**6**) was further confirmed by X-ray diffraction techniques. The electrochemical properties of complexes **1**, **2**, **5** and **6** were studied in dichloromethane solution. Complexes **1** and **2** display the reversible, four-membered, one-electron reduction sequence typical of fullerene ligands, as well as the reversible (in the cyclic voltammetric time scale) one-electron oxidation of the outer metal fragment. Complexes **5** and **6** are less stable to the same electron transfer processes. EPR measurements suggest that in the different electrogenerated monoanions, the added electrons enter the LUMO orbitals partially contributed by the metal fragment. In addition, they confirm that the instability of the reduction intermediates is due to the release of free C_{60}.

Introduction

The organotransition metal derivatives of C_{60} have drawn great attention[1] since the discovery of C_{60}[2] and its synthesis in macroscopic amounts.[3] The first example of such derivatives, namely (η^2-C_{60})Pt(PPh$_3$)$_2$, was reported in 1991 by Fagan and co-workers.[4] Although a great number of such derivatives have so far appeared in the literature,[5−8] very few organotransition metal C_{60} derivatives containing chiral ligands are known to be reported.[9,10] We have been interested in the synthesis, structural characterization and properties of organotransition metal fullerene complexes.[11] In view of the theoretical and practical significance of such complexes, we recently initiated a study on optically active organometallic C_{60} complexes. This paper describes the synthesis and spectroscopic characterization of the new optically active complexes *mer*-[(η^2-C_{60})M(CO)$_3${(−)-DIOP}] (**1**, M = Mo; **2**, M = W), *mer*-[(η^2-C_{60})M(CO)$_3${(+)-DIOP}] (**3**, M = Mo; **4**, M = W) and [(η^2-C_{60})M{(−)-DIOP}] (**5**, M = Pd; **6**, M = Pt), the crystal structure of **6** and the electrochemical properties of **1**, **2**, **5** and **6**.

[a] Department of Chemistry, State Key Laboratory of Elemento-Organic Chemistry, Nankai University,
Tianjin 300071, China
Fax: (internat.) + 86-22/23504853
E-mail: lcsong@public.tpt.tj.cn
[b] Dipartimento di Chimica dell'Università di Siena,
Via Aldo Moro, 53100 Siena, Italy

Results and Discussion

Synthesis and Characterization of *mer*-[(η^2-C_{60})M(CO)$_3$-{(−)-DIOP}] (1, M = Mo; 2, M = W) and *mer*-[(η^2-C_{60})M(CO)$_3${(+)-DIOP}] (3, M = Mo; 4, M = W)

Irradiation of [M(CO)$_6$] (M = Mo, W), in the presence of an equimolar quantity of C_{60} and (−)-DIOP or (+)-DIOP in chlorobenzene, with a UV 450-W mercury vapor lamp at ambient temperature, resulted in the formation of complexes **1**−**4** in 42−51% yields, as shown in Scheme 1.

Complexes **1**−**4** as the *mer* isomers obtained from the above "one-pot" reactions might be regarded as being produced by the reaction of M(CO)$_6$ with one of the chiral

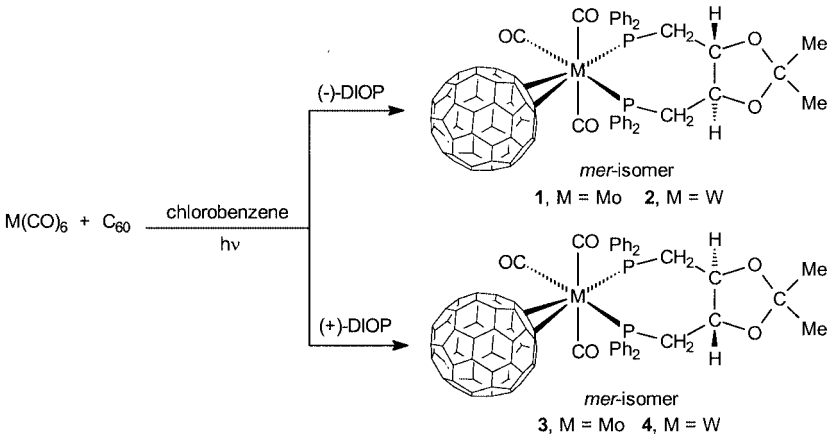

Scheme 1

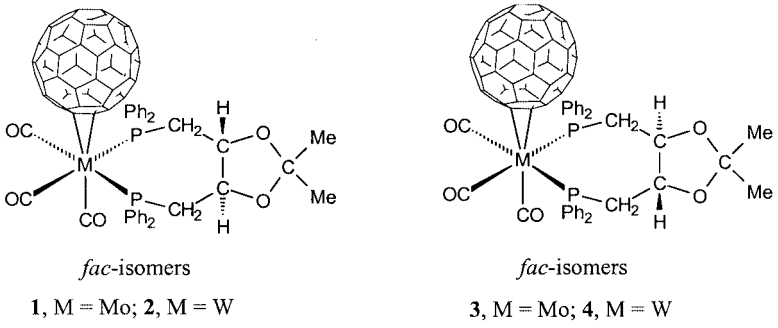

Scheme 2

diphosphane ligands (±)-DIOP, with subsequent substitution of one equatorial CO ligand from the intermediate complex [M(CO)$_4${(−)-DIOP}] or [M(CO)$_4${(+)-DIOP}] by the C_{60} ligand.

Complexes **1**−**4** are new and have been characterized by elemental analyses, ^{1}H (^{31}P, ^{13}C) NMR, UV/Vis, IR, FAB-MS and CD spectroscopy. The combustion analyses agree with their chemical formulas, and the FAB-MS spectra clearly show the molecular ion M^+ or [M^+ + 1 − 3 H] peaks. Theoretically, **1**−**4** each may have two possible isomers, namely the *fac* and the *mer* isomer. The *mer* isomers are shown in Scheme 1, and the *fac* isomers for **1**−**4** are shown in Scheme 2. However, the ^{31}P NMR spectra of **1**−**4** have indicated that they exist as the *mer* isomers. In the ^{31}P NMR spectra of **1**−**4**, two signals are present, which is consistent with the fact that *mer* isomers have two different P atoms, one *cis* to the C_{60} ligand, and the other *trans* to it (*fac* isomers have two identical P atoms, both *cis* to the C_{60} ligand). The two ^{31}P NMR signals are doublets; the doublets for the Mo complexes **1** and **3** appear at δ ≈ 20 and 15 ppm, with $J_{P\text{-}P}$ = 30−32 Hz, and the doublets for the W complexes **2** and **4** appear at δ ≈ −4 and −5 ppm, with $J_{P\text{-}P}$ ≈ 21 Hz. This can be seen from the two representative spectra of **3** and **4** (Figure 1). It is worth noting that the ^{31}P chemical shifts of complexes containing a DIOP ligand, such as **1**−**4**, usually lie at a higher field than the corre-

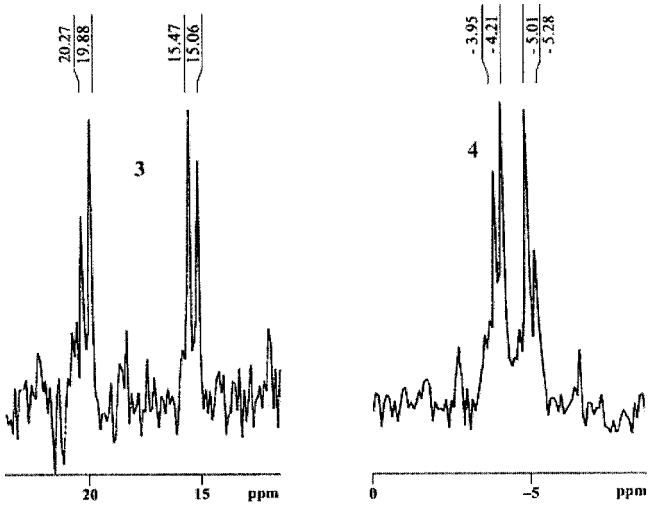

Figure 1. ^{31}P NMR spectra of **3** and **4**

sponding complexes containing a dppe ligand {such as *mer*-[$Mo(CO)_3$(dppe)(η^2-C_{60})] and *mer*-[$W(CO)_3$(dppe)(η^2-C_{60})]: δ_P = 62.64/54.21 ppm and 41.48/38.11 ppm, respectively} or a dppb ligand {such as *mer*-[$Mo(CO)_3$(dppb)(η^2-C_{60})] and *mer*-[$W(CO)_3$(dppb)(η^2-C_{60})]: δ_P = 66.18/55.66 ppm and 49.50/43.49 ppm, respectively}. This is because δ_P of the free ligand DIOP (δ = −23.5 ppm)[12] lies at a much higher field than those of the free ligands dppe (δ = 12.5 ppm)[13] and dppb (δ = −13.41 ppm, determined by us, since no reported δ_P value is available).

The ^{1}H NMR spectra of **1**−**4** are much more complicated than those of the free ligands (−)-DIOP and (+)-DIOP. The spectra of the free ligands show a sharp singlet assigned to the two methyl groups. This singlet appears as two singlets in the spectra of their complexes. The two broad peaks in the spectra of the free DIOP ligands, assigned to the two H atoms bonded to the chiral carbon atoms, appear as two apparent triplets and two apparent quadruplets in the spectra of their complexes. Further, in the spectra of the free ligands, the multiplet assigned to the two CH_2 groups, appears as two multiplets in the spectra of their complexes. Obviously, such ^{1}H NMR spectroscopic changes are consistent with the chelation of the DIOP ligands in the *mer*-isomers of **1**−**4**.

In the ^{13}C NMR spectra of **1**−**4**, the saturated, ketal and phenyl ring carbon atoms of the DIOP ligands lie in the ranges δ = 17−27, 103−109 and 123−136 ppm, respectively. In addition, the C_{60} ligands in **1**−**4** display resonance signals in the ranges δ = 136−163 ppm for the 58 sp^2 carbon atoms, and δ = 73−80 ppm for their 2 sp^3 carbon atoms. This is consistent with known η^2-C_{60} transition metal complexes, such as [$Rh(NO)(PPh_3)_2$(η^2-C_{60})][14] and [$Fe(CO)_4$(η^2-C_{60})].[15] The ^{13}C NMR spectrum of the sp^2 and sp^3 carbon atoms of the C_{60} core in **2** is shown in Figure 2. As seen in Figure 2, there are 20 signals in the δ = 164−140 ppm region, which can be assigned to the 58 carbon atoms of the C_{60} core.[14,15] Another ^{13}C NMR signal at δ = 78.81 ppm can be assigned to the two sp^3 carbon atoms of the C_{60} core that is directly linked to the W atom.[14,15] Among the 20 signals, two signals at δ = 163.43 and 162.78 ppm are assigned to the four carbon atoms in close proximity to the carbon atoms linked to the W atom. Nine signals at δ = 147.09, 145.40, 145.05, 144.44, 144.35, 142.59, 142.49, 142.01 and 141.77 ppm can each be assigned to four carbon atoms and the other eleven signals at δ = 163.43, 162.78, 146.27, 145.28, 144.86, 143.87, 143.77, 143.64, 142.92, 141.33 and 140.03 ppm can each be assigned to two carbon atoms. Similarly, in the ^{13}C NMR spectrum of the C_{60} core, **1** displays 25 signals in the region δ = 163.42−140.95 ppm and one signal at δ = 80.01 ppm, **3** shows 19 signals in the region δ = 163.03−140.56 ppm and one signal at δ = 78.72 ppm, and **4** exhibits 22 signals in the region δ = 158.21−136.55 ppm and one signal at δ = 73.60 ppm.

The IR spectra of **1**−**4** show four characteristic absorption bands for the C_{60} core[16] in the range 1434−525 cm^{-1}, as well as three strong bands in the range 2002−1870 cm^{-1}, which can be assigned to the terminal carbonyl groups.[17] The simplicity of the carbonyl bands provides further evidence that complexes **1**−**4** consist of only one isomer (since a mixture of *fac*/*mer* isomers would exhibit more active carbonyl absorption bands).[18]

In the UV/Vis spectra of **1**−**4**, there are five absorbance bands in the range 200−610 nm. This is typical of a free C_{60} ligand that has been complexed by a transition metal moiety.[19] The largest changes in the UV/Vis spectra occur in the visible region relative to that of free C_{60}. A new weak and broad band appears at ca. 430 nm in the spectra of complexes **1**−**4**. This peak is responsible for the color change in the reaction mixture, from purple C_{60} to dark green for the corresponding complexes. In addition, the new band suggests that the C_{60} ligands are coordinated to Mo and W atoms via an η^2-coordination mode in **1**−**4**.[20]

CD spectroscopy is an important method for the characterization of chiral compounds. The CD spectra of **1**−**4** are shown in Figures 3 and 4, respectively. As can be seen in Figure 3, **1** shows the negative and positive Cotton effects at 293 (−), 326 (+), 401 (−), 451 (−) and 540 (+) nm, and **2** displays similar Cotton effects at 288 (−), 324 (+), 399 (−), 449 (−) and 537 (+) nm.

Interestingly, the CD spectra of **3** and **4** (Figure 4) appear to be the mirror images of **1** and **2**, respectively. For example, **3** shows Cotton effects at 293 (+), 326(−), 402 (+), 450 (+), and 538 (−) nm, whereas **1** shows Cotton effects at 293 (−), 326(+), 401 (−), 451 (−) and 540 (+) nm. This is consistent with the behavior of chiral compounds with the ligands (+)-DIOP and (−)-DIOP. In addition, it is worth noting that the main Cotton effects of **3** and **4**, con-

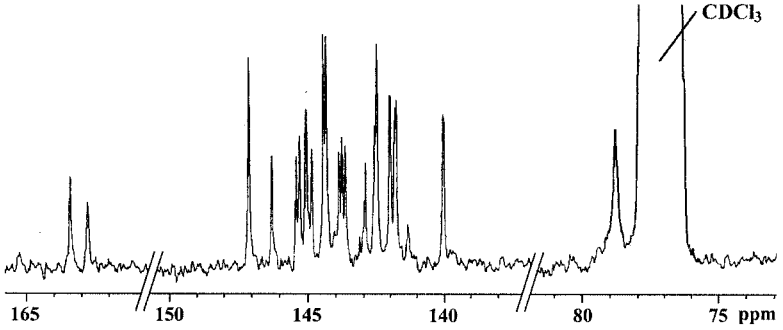

Figure 2. ^{13}C NMR spectrum of the C_{60} core in **2**

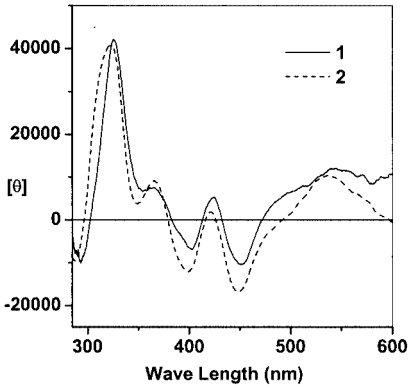

Figure 3. CD spectra of complexes **1** and **2** in THF

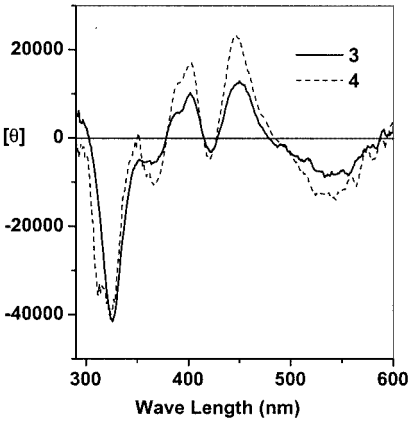

Figure 4. CD spectra of complexes **3** and **4** in THF

taining a (+)-DIOP ligand, are very similar to those of (η^2-C_{60})Pt{(+)-DIOP} and (η^2-C_{60})Pd{(+)-DIOP}.[21]

Electrochemistry of Complexes 1 and 2 and Complementary EPR Measurements

Figure 5 shows the cyclic voltammetric behavior of the W complex **2** in dichloromethane solution at −20 °C.

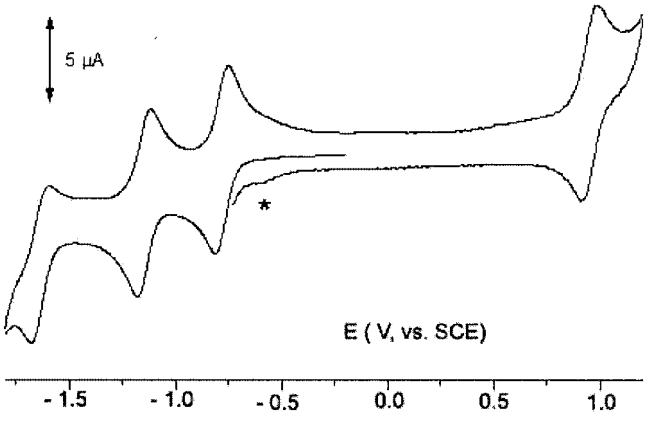

Figure 5. Cyclic voltammogram on a platinum electrode of a CH_2Cl_2 solution of **2** (0.4×10^{-3} mol·dm^{-3}); scan rate 0.2 V·s^{-1}; $T = -20$ °C; the starred peak indicates the appearance of identified by-products (see text)

Three sequential reductions appear that have features indicating chemical (i_{pa}/i_{pc} constantly equal to 1, independently from scan rate) and electrochemical (ΔE_p in the range from 58 to 70 mV with scan rate varying from 0.02 V·s^{-1} to 0.5 V·s^{-1}) reversibility. An oxidation process also occurs that shows reversibility.

In confirmation with the suggested fullerene-centered nature of the cathodic processes and their chemical reversibility, controlled potential coulometry of the first reduction step ($E_w = -0.9$ V) indicates one electron per molecule. The resulting solution displays a cyclic voltammetric profile that resembles the original one.

The anodic process is straightforwardly assigned as a one-electron process that is centered on the exohedral metal fragment. In spite of its features, which show chemical reversibility, it can be seen that in the back-scan a minor starred-peak appears at potential values coincident with the first reduction process of the free fullerene. This suggests that the monocation $[\mathbf{2}]^+$ is not indefinitely stable. At ambient temperature, the voltammetric patterns remain substantially unaltered.

The formal electrode potentials of the multiple redox changes are presented in Table 1.

As commonly seen for metallofullerenes,[22] the reduction processes are shifted towards more negative potential values, indicating that the appended metal fragment is electron-donating towards the fullerene. In the present case, these values are shifted by about 0.20 V with respect to the free fullerene.

In previous papers we have proved, by EPR spectroscopy, that the LUMO orbitals of exohedral metallofullerenes are in part contributed by the d orbitals of the metal ion itself.[23] Here, we have studied the nature of the electrogenerated paramagnetic anion radical $[\mathbf{2}]^-$ by X-band EPR spectroscopy. Figure 6 shows the spectrum recorded under glassy conditions ($T = 100$ K), relative to that of $[C_{60}]^-$.

The broad lineshape of $[\mathbf{2}]^-$ can be suitably interpreted assuming an $S = 1/2$ electron spin Hamiltonian with axial resolution either in the first or second derivative modes. The EPR features suggest that the paramagnetic species possesses significant metallic character [$g_i > g_{electron} = 2.0023$; $\Delta g = 0.083(5)$]. No evidence for a_{aniso} hyperfine (hpf) splittings of the ^{183}W nucleus (^{183}W: I nuclear spin = 1/2; natural abundance = 14.4%) has been obtained, probably as a consequence of either the broad lineshape, which masks the low intensity satellite peaks of the ^{183}W isotope, or the partial metallic character.[23] Moreover, no ^{31}P (^{31}P: $I = 1/2$; natural abundance = 100%) superhyperfine (shpf) splittings are detectable in the second derivative mode, suggesting that the unpaired electron is mainly delocalized in a SOMO basically constituted by the C_{60} and metal d atomic orbitals.

When the temperature at the glassy-fluid transition phase is raised, the anisotropic features of $[\mathbf{2}]^-$ disappear and the fluid solution becomes EPR-silent. However, rapid refreezing quantitatively restores the original glassy spectrum. This indicates the stability of the metal complex species under different experimental conditions. The absence of the absorption peaks under fluid solution conditions is not un-

Table 1. Formal electrode potentials (V, vs. SCE) and peak-to-peak separation (mV) for the redox changes exhibited by *mer*-[(η^2-C_{60})M(CO)$_3${(−)-DIOP}] (**1**, M = Mo; **2**, M = W) in CH_2Cl_2 solution at −20 °C

Complex (M)	Fullerene-centered reductions						Metal-centered oxidation	
	$E^{\circ\prime}_{0/-}$	ΔE_p [a]	$E^{\circ\prime}_{-/2-}$	ΔE_p [a]	$E^{\circ\prime}_{2-/3-}$	ΔE_p [a]	$E^{\circ\prime}_{0/+}$	ΔE_p [a]
1 (Mo)	−0.76	62	−1.11	62	−1.60	70	+0.88	64
2 (W)	−0.78	62	−1.15	60	−1.65	58	+0.95[b]	60
C_{60}	−0.58	62	−0.96	64	−1.42	60	−	−

[a] Measured at 0.1 Vs^{-1}. [b] Coupled to relatively slow chemical complications.

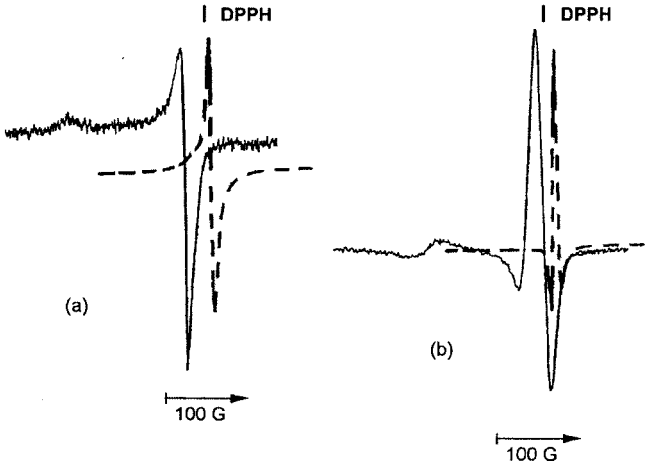

Figure 6. Low-temperature (T = 105 K) X-band EPR spectra of the electrogenerated anions [**2**]$^-$ (——) and [C_{60}]$^-$ (− −) in CH_2Cl_2 solution; (a) first derivative; (b) second derivative

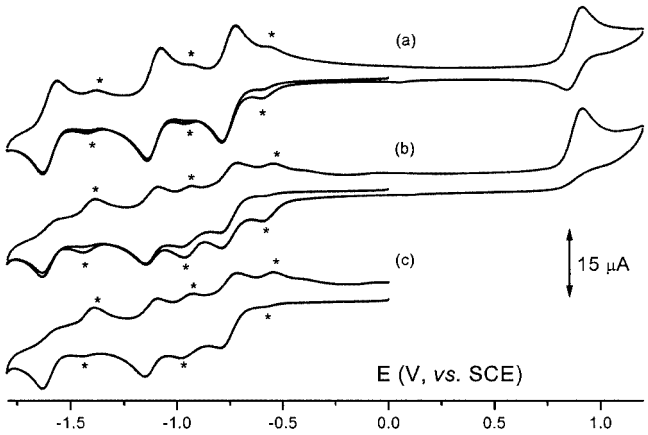

Figure 7. Cyclic voltammograms on a platinum electrode of a CH_2Cl_2 solution of **1** (0.7×10^{-3} mol·dm^{-3}); (a) T = −20 °C; (b, c) T = +20 °C; scan rate 0.2 V·s^{-1}; starred peaks indicate the appearance of identified by-products (see text)

expected in view of the increasing inter-/intramolecular dynamics induced by temperature. This in turn reflects the significant decrease in the ESR times.[24]

The X-band EPR parameters obtained by simulation procedures[25] are presented in Table 2.

Table 2. Low-temperature (100 K) X-band EPR parameters of the electrogenerated anions [2]$^-$ and [C_{60}]$^-$ in CH_2Cl_2 solution (g_i: ± *0.005)*

Anion	$g_\parallel$	$g_\perp$	$<g>$[a]	g_{iso}
[**2**]$^-$	2.093	2.010	2.034	−
[C_{60}]$^-$	2.006[b]	2.006[b]	2.006[b]	2.001[c]

[a] $<g> = (g_\parallel + 2g_\perp)/3$. [b] Averaged values. [c] T = 230 K.

The redox activity of the molybdenum analogue **1** is illustrated in Figure 7.

At low temperatures (T = −20 °C), **1** exhibits a voltammogram that is similar to that of **2** (Figure 7, a). In fact, apart from minor traces of free C_{60} initially present in solution, three fullerene-centered reductions also appear that have features indicative of chemical and electrochemical reversibility. In this case, however, the molybdenum-centered oxidation is partially chemically reversible (i_{pc}/i_{pa} = 0.4 at 0.1 V·s^{-1}). The fact that the instability of [**1**]$^+$ is due to the relatively fast release of the fullerene subunit can clearly be seen from the voltammogram in Figure 7 (b), which has been recorded at ambient temperature. Increasing amounts of the free fullerene are evident in the backscan, indicated as starred reduction processes. However, it should be noted that the monoanions [**1**]$^{-/2-/3-}$ are unstable at increasing temperatures, such that the fast release of free C_{60} occurs after traversing the respective peaks (Figure 7, c). The pertinent formal electrode potentials are given in Table 1.

Synthesis and Characterization of [(η^2-C_{60})M{(−)-DIOP}] (5, M = Pd; 6, M = Pt)

The toluene solution of the intermediate complex [(η^2-C_{60})Pd(PPh_3)$_2$] or [(η^2-C_{60})Pt(PPh_3)$_2$], formed from C_{60} and [Pd(PPh_3)$_4$] or [Pt(PPh_3)$_4$], reacted in situ with an excess amount of (−)-DIOP, through a ligand exchange process between PPh_3 and DIOP, to give **5** and **6**, as shown in Scheme 3.

Complexes **5** and **6** were isolated, as their toluene solvates **5**·PhMe and **6**·PhMe in > 90% yields, by layering the reaction mixtures with hexane.

Compounds **5** and **6** were fully characterized by elemental analysis, ^{1}H, ^{31}P NMR, IR and UV/Vis spectroscopy. The ^{31}P NMR spectrum of **5** displays a singlet at δ = 9.28 ppm assigned to its two identical P atoms, and that of **6** exhibits a singlet at δ = 11.13 ppm, along with two satellite singlets due to the ^{195}Pt-^{31}P coupling, assigned to its two identical P atoms. The Pt-P coupling constant (3749 Hz) for **6** is almost the same as that for [(η^2-C_{60})Pt{(+)-DIOP}] (3751 Hz).[10] The ^{1}H NMR spectra of

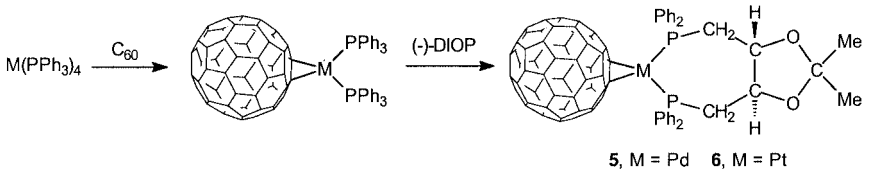

Scheme 3

5 and **6** indicate the presence of the (−)-DIOP ligand and toluene as the solvent molecule.

Compared with the UV/Vis spectrum of free C_{60}, the UV/Vis spectra of **5** and **6** display a new band at ca. 295 nm in the ultraviolet region, and a new band at 440 nm in the visible region. The former band can be attributed to the presence of phenyl groups in **5** and **6**, and the latter to the η^2-coordinating mode of C_{60} [20] with Pd and Pt, in **5** and **6**, respectively. The IR spectra of **5** and **6** show four absorption bands at 527, 576, 1184 and 1428 cm^{-1}, characteristic of the C_{60} core.

Interestingly, similar to the Mo/W complexes **1**−**4**, the CD spectra of **5** and **6**, as shown in Figure 8, display multiple Cotton effects at 298 (+), 325 (−), 366 (−) and 453 (+) nm for **5**, and 291 (+), 324 (−), 363 (−) and 450 (+) nm for **6**. The CD spectra of **5** and **6** are the mirror images of their enantiomers with (+)-DIOP in the region 280−600 nm.[21]

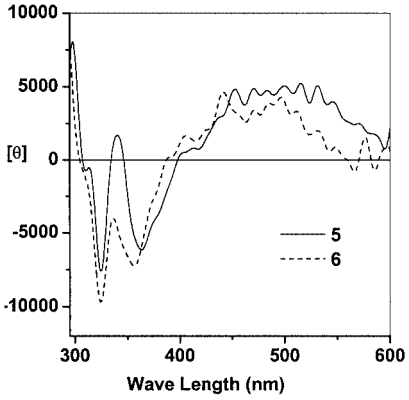

Figure 8. CD spectra of complexes **5** and **6** in toluene

Single Crystal Molecular Structure of 6

The structure of **6** has been unambiguously confirmed by X-ray diffraction methods. The molecular structure of **6** and its cell packing are demonstrated in Figures 9 and 10, respectively. As seen intuitively from Figure 9, complex **6** consists of a (4*R*,5*R*)-DIOP [i.e. (−)-DIOP] ligand chelated to platinum atom Pt(1) through its two phosphorous atoms P(1) and P(2), and a C_{60} ligand coordinated to Pt(1) through its C(1) and C(2) atoms in an η^2-fashion. The C(1)−C(2) bond length is 1.502(11) Å, similar to that of a normal C−C single bond, which suggests that C(1) and C(2) are σ-coordinated rather than π-coordinated to form a metallacyclopropane ring with the Pt(1) atom. The zerovalent platinum atom Pt(1) is at the center of a tetragon

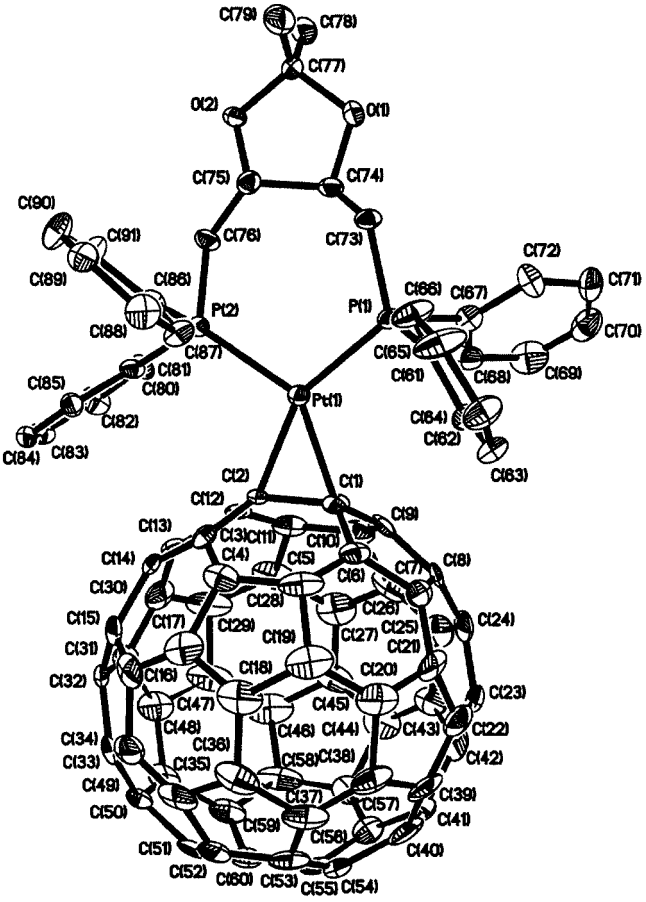

Figure 9. Structural drawing of **6** with ellipsoids drawn at the 30% probability

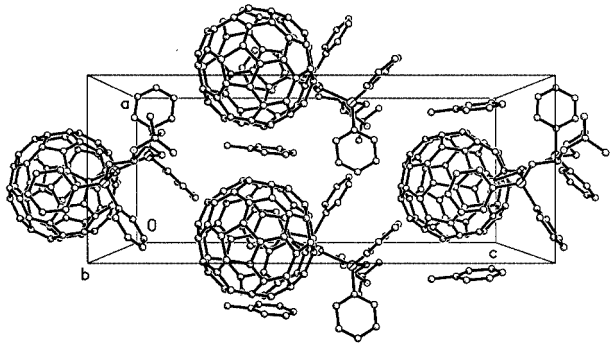

Figure 10. Molecular arrangement in a unit cell of **6**

constituted by the atoms C(1), C(2), P(1) and P(2), and all five atoms are coplanar with a mean deviation of only 0.014 Å. In addition, it is worth noting that the C_{60} ligand in **6** is slightly distorted from the perfect sphere. The two coordin-

ating carbon atoms C(1) and C(2) are pulled out of the spherical surface by about 0.2 Å, and the distance from C(1) and C(2) to the C_{60} center (ca. 3.72 Å) is much longer than the distance from each of the other carbon atoms to the C_{60} center (3.49−3.56 Å). As a matter of fact, such a structure is typical of some diphosphane-chelated C_{60} transition metal complexes. Table 3 shows some geometric parameters of the crystal structures of **6** and its enantiomer (η^2-C_{60})Pt{(+)-DIOP}.[10] Obviously, the geometric parameters of these two platinum complexes are very similar to each other.

Table 3. Comparison of the crystal structures of **6** and its analogue with (+)-DIOP

	6	(η^2-C_{60})Pt{(+)-DIOP}
Bond length between the two coordinating carbon atoms [Å]	1.502(11)	1.51(2)
Pt−C bond length [Å]	2.107(7)	2.09(2)
	2.135(7)	2.12(2)
Pt−P bond length [Å]	2.252(2)	2.262(4)
	2.281(2)	2.279(4)
C−Pt−C bond angle [°]	41.5(3)	42.0(4)
P−Pt−P bond angle [°]	105.41(7)	109.47(13)
C−Pt−P bond angle [°]	101.2(2)	104.2(4)
	111.8(2)	104.4(4)

As seen in Figure 10, each crystal cell contains four molecules of **6** and four molecules of toluene. The closest distance between the solvent molecule toluene and the C_{60} moiety in **6** is 3.6 Å. This indicates that there are no evident interactions between them.

Electrochemistry of Complexes 5 and 6 and Complementary EPR Measurements

As exemplified in Figure 11 which refers to the Pt complex **6**, derivatives [(η^2-C_{60})M{(−)-DIOP}] exhibit a reduced redox activity compared with that of [(η^2-C_{60})M(CO)$_3${(−)-DIOP}].

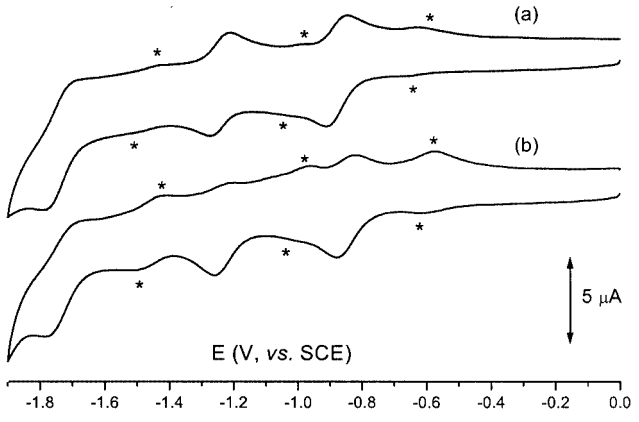

Figure 11. Cyclic voltammograms on a platinum electrode of a CH_2Cl_2 solution of **6** (0.7×10^{-3} mol·dm^{-3}); (a) $T = -20$ °C; (b) $T = +20$ °C; scan rate 0.2 V s^{-1}; starred peaks indicate the appearance of identified by-products (see text)

Complexes **5** and **6** display two fullerene-centered sequential reductions. The reduction processes show significant chemical reversibility, only at low temperatures. At ambient temperature, fast release of free C_{60} occurs on reduction. A third cathodic process is present at very negative potential values, which, based on the relative peak-height, most likely involves the metal fragment.[23] Further, these complexes show an anodic process (not shown in figure) that is completely irreversible (or, quick C_{60} release take places) at low temperatures. The formal electrode potentials are presented in Table 4.

It should be noted that the Pd/Pt fragment is slightly more electron-donating than the Mo/W unit, such that the negative shift in the redox potentials is about 0.25 V with respect to the free fullerene.

In agreement with the electrochemical findings, the liquid-nitrogen X-band EPR spectra of the electrogenerated [**5**]$^-$ monoanion show the undoubted presence of [C_{60}]$^-$ (Figure 12).

As a matter of fact, two different paramagnetic species, partially overlapped in the high-field region, are detected. The narrow, high-field (starred) signal is due to the [C_{60}]$^-$ monoanion, while the low-field signal is attributed to the parallel region of the axial absorption of [**5**]$^-$, the relevant broad parallel region is shifted at lower field. The metallofullerene anion exhibits significant metallic character [$g_i > g_{electron} = 2.0023$; $\Delta g = 0.090(5)$]. There is no evidence for a_{aniso} hpf splittings of the ^{105}Pd nucleus (^{105}Pd: I nuclear spin = 5/2; natural abundance = 22.2%), as well as no ^{31}P shpf splittings. When the temperature at the glassy-fluid transition is raised, the anisotropic features of [**5**]$^-$ disappear, while the isotropic signal of the [C_{60}]$^-$ monoanion is maintained. Rapidly refreezing the fluid solution quantitatively restores the original glassy spectrum of the complex. The X-band EPR parameters are given in Table 5.

In spite of the apparent high stability of the Pt anion [**6**]$^-$ in the cyclic voltammetric time scale, exhaustive electrolysis at the first cathodic process of **6** affords a solution which, through EPR spectroscopy, only shows the signal for [C_{60}]$^-$.

Experimental Section

General: All reactions were carried out under highly purified nitrogen using standard Schlenk or vacuum-line techniques. Chlorobenzene was dried by distillation from P_2O_5 and subsequently from CaH_2 under nitrogen. Toluene, THF, pentane and hexane were distilled under nitrogen from sodium/benzophenone ketyl. All solvents were degassed by bubbling a stream of nitrogen through them for at least 15 min before use. C_{60} (99.9%), (−)-DIOP and (+)-DIOP were of commercial grade and used as received. [$Pd(PPh_3)_4$][26] and [$Pt(PPh_3)_4$][27] were prepared according to literature procedures. Preparative thin-layer chromatography (TLC) and column chromatography were performed on glass plates coated with silica gel (10−40 μm, 20 cm × 25 cm × 0.25 cm) and glass columns packed with silica gel (200−300 mesh, 30 cm × 2.5 cm), respectively. Melting points were determined with a Yanaco MP-500 melting point apparatus. Elemental analyses and FAB-MS were performed with

Table 4. Formal electrode potentials (V, vs. SCE) and peak-to-peak separation (mV) for the redox changes exhibited by (η^2-C_{60})M{(−)-DIOP} (**5**, M = Pd; **6**, M = Pt) in CH_2Cl_2 solution at −20 °C

Complex (M)	Fullerene-centered reductions				Metal-centered oxidation
	$E^{\circ\prime}_{0/-}$	ΔE_p [a]	$E^{\circ\prime}_{-/2-}$	ΔE_p [a]	E_p[b]
5 (Pd)	−0.83	56	−1.19	56	+0.66
6 (Pt)	−0.84	64	−1.24	63	+0.74
C_{60}	−0.58	62	−0.96	64	−

[a] Measured at 0.1 V·s^{-1}. [b] Peak potentials for irreversible processes.

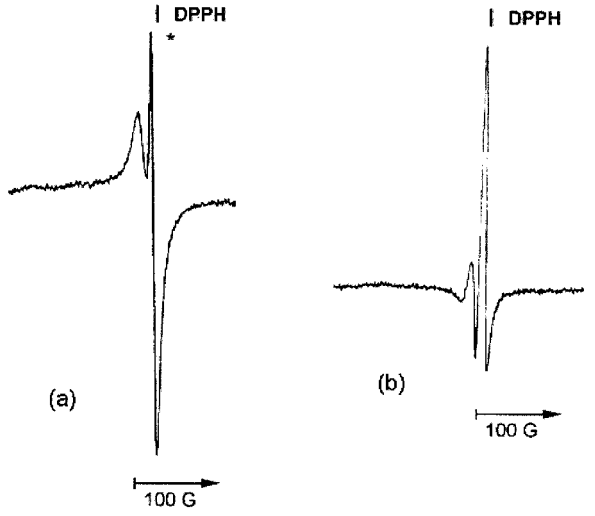

Figure 12. Low-temperature (T = 105 K) X-band EPR spectra of the solution electrogenerated at the first reduction process of **5** in CH_2Cl_2 solution; (a) first derivative; (b) second derivative

Table 5. Low-temperature (100 K) X-band EPR parameters of the electrogenerated anions $[5]^-$ in CH_2Cl_2 solution (g_i: ± 0.005)

Anion	$g_\parallel$	$g_\perp$	$<g>$	g_{iso}[a]
$[\mathbf{5}]^-$	2.094	2.004	2.038	−
$[C_{60}]^-$	2.006[b]	2.006[b]	2.006[b]	2.001[c]

[a] $<g> = (g_\parallel + 2g_\perp)/3$. [b] Averaged values. [c] T = 230 K.

an Elementar Vario EL analyzer and a Zabspec spectrometer, respectively. IR and UV/Vis spectra were recorded with a Bio-Rad FTS-135 and a Shimadzu UV-2401/PC spectrophotometer, respectively. ^{1}H NMR, ^{31}P NMR and ^{13}C NMR spectra were obtained either with a Bruker AC-P200 or a UNITY-PLUS 400 spectrometer. The CD spectra and the specific rotatory powers were determined with a JASCO 715 spectrapolarimeter and a Perkin−Elmer 241-MC polarimeter, respectively. Materials and apparatus for electrochemistry and joint EPR spectroscopy have been described elsewhere.[23] Potential values are referred to the saturated calomel electrode (SCE). Under the present experimental conditions, the one-electron oxidation of ferrocene occurs at +0.36 V.

Preparation of *mer*-[(η^2-C_{60})Mo(CO)$_3${(−)-DIOP}] (1): A 100-mL photoreactor equipped with an N_2 inlet tube and a serum cap was charged with C_{60} (0.072 g, 0.10 mmol), (−)-DIOP (0.050 g, 0.10 mmol), [Mo(CO)$_6$] (0.026 g, 0.10 mmol) and chlorobenzene (50 mL). The mixture was sonicated until all C_{60} was dissolved. The photoreactor containing the resulting purple solution was evacuated to a pressure of ca. 0.1 Torr, and was irradiated by a water-cooled UV 450-W mercury vapor lamp for 3 h to afford a dark green solution. The resulting solution was concentrated in vacuo, and the residue was separated by column chromatography using toluene/light petroleum ether (2:1, v/v) as the eluent under anaerobic conditions. From the second chlorophyll-green band, 0.059 g (42%) of **1** as a dark green solid was obtained. M.p. 300 °C (dec.). ^{1}H NMR (400 MHz, $CDCl_3$): δ = 1.35 (s, 3 H, CH_3), 1.46 (s, 3 H, CH_3), 1.60−1.88 (m, 2 H, CH_2), 2.35 (q, J = 8 Hz, 0.5 H, OCH), 3.01 (t, J = 13.2 Hz, 0.5 H, OCH), 3.26 (t, J = 13.2 Hz, 0.5 H, OCH), 3.62−3.78 (m, 2 H, CH_2), 4.93 (q, J = 8 Hz, 0.5 H, OCH), 7.10−8.00 (m, 20 H, 4 C_6H_5) ppm. ^{31}P NMR (80.96 MHz, $CDCl_3$): δ = 20.05 (d, 1 P), 15.26 (d, $J_{P\text{-}P}$ = 29.6 Hz, 1 P) ppm. ^{13}C{^{1}H} NMR (100.6 MHz, C_6D_6): δ = 211.17 (CO), 210.48 (CO), 163.42 (2 C), 162.76 (2 C), 147.59 (2 C), 147.54 (2 C), 146.63 (2 C), 146.04 (2 C), 145.93 (2 C), 145.82 (2 C), 145.67 (4 C), 145.11 (4 C), 145.04 (4 C), 144.76 (2 C), 144.70 (2 C), 144.59 (2 C), 144.05 (2 C), 143.69 (2 C), 143.62 (2 C), 143.38 (4 C), 142.97 (2 C), 142.89 (2 C), 142.75 (2 C), 142.67 (2 C), 142.30 (2 C), 141.10 (2 C), 140.95 (2 C), 80.01 (2 C) (C_{60} resonance), 135.2, 134.65, 134.45, 134.34, 133.09, 132.99, 131.62, 131.44, 131.02, 130.91, 130.81, 130.28, 129.73, 129.64, 129.51, 129.42 (4 C_6H_5P, resonance), 109.28 (−OCO−), 27.47 (CHO), 27.39 (CH_2), 23.07 (CH_3) ppm. IR (KBr disk): $\tilde{\nu}$ = 2002 (s), 1943 (s), 1883 (vs) (C≡O), 1434 (m), 1185 (w), 586 (w), 526 (s) (C_{60}) cm^{-1}. MS (FAB): m/z = 720 [C_{60}^+], 1401 {[M + H]$^+$, ^{98}Mo}. UV/Vis (THF) λ_{max} (log ε) = 237.9 (5.07), 257.1 (5.21), 330.7 (4.65), 433.9 (4.20), 600.5 (3.87) nm. $[\alpha]^{25}_{365}$ = +2.7 (c = 3.15 × 10^{-5} mol/L, THF). $C_{94}H_{32}MoO_5P_2$ (1399.17): calcd. C 80.69, H 2.31; found C 80.40, H 2.55.

***mer*-[(η^2-C_{60})W(CO)$_3${(−)-DIOP}] (2):** The same synthetic procedure was employed as for the preparation of **1**, except that [W(CO)$_6$] (0.035 g, 0.10 mmol) was used instead of the molybdenum complex [Mo(CO)$_6$], and the reaction mixture was separated by TLC using toluene/light petroleum ether (2:1, v/v) as the eluent under anaerobic conditions. From the second chlorophyll-green band, 0.076 g (51%) of **2** as a dark green solid was obtained. M.p. 300 °C (dec.). ^{1}H NMR (200 MHz, $CDCl_3$): δ = 1.33 (s, 3 H, CH_3), 1.45 (s, 3 H, CH_3), 1.72−2.00 (m, 2 H, CH_2), 2.40 (q, J = 8 Hz, 0.5 H, OCH), 3.22 (t, J = 13.2 Hz, 0.5 H, OCH), 3.39(t, J = 13.2 Hz, 0.5 H, OCH), 3.70−3.92 (m, 2 H, CH_2), 4.91 (q, J = 8 Hz, 0.5 H, OCH), 7.12−8.12 (m, 20 H, 4 C_6H_5) ppm. ^{31}P NMR (80.96 MHz, $CDCl_3$): δ = −3.97 (d, 1 P), −5.14 (d, $J_{P\text{-}P}$ = 21.5 Hz, 1 P) ppm. ^{13}C{^{1}H} NMR (100.6 MHz, $CDCl_3$): δ = 203.52 (CO), 202.58 (CO), 163.43 (2 C), 162.78 (2 C), 147.09 (4 C), 146.27 (2 C), 145.40 (4 C), 145.28 (2 C), 145.05 (4 C), 144.86 (2 C), 144.44 (4 C), 144.35 (4 C), 143.87 (2 C), 143.77 (2 C), 143.64 (2 C), 142.92

(2 C), 142.59 (4 C), 142.49 (4 C), 142.01 (4 C), 141.77 (4 C), 141.33 (2 C), 140.03 (2 C), 78.81 (2 C) (C_{60} resonance), 134.43, 133.95, 133.83, 132.61, 132.34, 132.25, 131.54, 131.35, 130.73, 130.50, 130.41, 130.25, 129.11, 128.49, 128.40 (4 C_6H_5P, resonance), 108.84 (−OCO−), 26.95 (CHO), 26.84 (CH_2), 21.71 (CH_3) ppm. IR (KBr disk): $\tilde{\nu}$ = 2000 (s), 1938 (s), 1870 (vs) (C≡O), 1434 (m), 1186 (w), 584 (w), 526 (s) (C_{60}) cm^{-1}. MS (FAB): *m*/*z* = 720 (C_{60}^{+}), 1491 {[M + 3 H]$^+$, ^{186}W}. UV/Vis (THF): λ_{max} (log ε) = 239.3 (5.06), 256.9 (5.11), 340.5 (4.61), 429.5 (4.25), 592.1 (3.88) nm. $[\alpha]_{365}^{25}$ = +4.4 ($c = 2.16 \times 10^{-5}$ mol/L, THF). $C_{94}H_{32}O_5P_2W$ (1487.08): calcd. C 75.92, H 2.17; found C 75.80, H 2.49.

***mer*-[(η²-C_{60})Mo(CO)$_3${(+)-DIOP}] (3):** The same synthetic procedure was employed as for the preparation of **1**, except that (+)-DIOP (0.050 g, 0.10 mmol) was used instead of (−)-DIOP. The reaction mixture was separated by TLC using toluene/light petroleum ether (6:1, v/v) as the eluent under anaerobic conditions. From the second chlorophyll-green band, 0.068 g (48%) of **3** as a dark green solid was obtained. M.p. 300 °C (dec.). ^{1}H NMR (200 MHz, $CDCl_3$): δ = 1.32 (s, 3 H, CH_3), 1.43 (s, 3 H, CH_3), 1.60−1.90 (m, 2 H, CH_2), 2.30 (q, *J* = 8 Hz, 0.5 H, OCH), 3.00 (t, *J* = 16 Hz, 0.5 H, OCH), 3.30 (t, *J* = 16 Hz, 0.5 H, OCH), 3.60−3.80 (m, 2 H, CH_2), 4.90 (q, *J* = 8 Hz, 0.5 H, OCH), 7.10−8.00 (m, 20 H, 4 C_6H_5) ppm. ^{31}P NMR (80.96 MHz, $CDCl_3$): δ = 20.07 (d, 1 P), 15.27 (d, $J_{P\text{-}P}$ = 32.1 Hz, 1 P) ppm. ^{13}C{^{1}H} NMR(100.6 MHz, $CDCl_3$): δ = 163.03 (2 C), 162.43 (2 C), 147.24 (4 C), 146.39 (2 C), 145.82 (2 C), 145.70 (2 C), 145.49 (2 C), 145.36 (2 C), 144.89 (4 C), 144.80 (4 C), 144.35 (4 C), 144.19 (2 C), 143.71 (8 C), 143.40 (2 C), 143.10 (4 C), 142.68 (4 C), 142.48 (4 C), 140.67 (2 C), 140.56 (2 C), 78.72 (2 C) (C_{60} resonance), 136.22, 134.90, 134.58, 134.40, 134.02, 133.10, 131.81, 131.60, 130.97, 130.54, 129.69, 129.53, 129.21, 129.05, 128.46, 128.21 (4 C_6H_5P, resonance), 109.25 (−OCO−), 27.26 (CHO), 26.76 (CH_2), 22.79 (CH_3) ppm. IR (KBr disk): $\tilde{\nu}$ = 1997 (s), 1934 (s), 1882 (vs, C≡O), , 1430 [m, ν(C_{60})], 1185 (w), 584 (w), 523 (s, C_{60}) cm^{-1}. MS (FAB): *m*/*z* = 1395 {[M$^+$], ^{92}Mo}. UV/Vis (THF): λ_{max} (log ε) = 252.5 (5.07), 290.0 (4.80), 328.0 (4.71), 436.0 (4.23), 605.0 (3.72) nm. $[\alpha]_{365}^{25}$ = −3.74 ($c = 3.06 \times 10^{-5}$ mol/L, THF). $C_{94}H_{32}MoO_5P_2$ (1399.17): calcd. C 80.69, H 2.31; found C 80.43, H 2.60.

***mer*-[(η²-C_{60})W(CO)$_3${(+)-DIOP}] (4):** The same synthetic procedure was employed as for the preparation of **3**, except that [W(CO)$_6$] (0.035 g, 0.10 mmol) was used instead of [Mo(CO)$_6$], and the reaction mixture was separated by TLC using toluene/light petroleum ether (6:1, v/v) as the eluent under anaerobic conditions. From the second chlorophyll-green band, 0.065 g (43%) of **4** as a dark green solid was obtained. M.p. 300 °C (dec.). ^{1}H NMR (200 MHz, $CDCl_3$): δ = 1.33 (s, 3 H, CH_3), 1.45 (s, 3 H, CH_3), 1.65−1.90 (m, 2 H, CH_2), 2.40 (q, *J* = 8 Hz, 0.5 H, OCH), 3.20(t, *J* = 12 Hz, 0.5 H, OCH), 3.40 (t, *J* = 12 Hz, 0.5 H, OCH), 3.80−4.00 (m, 2 H, CH_2), 4.95 (q, *J* = 8 Hz, 0.5 H, OCH), 7.10−8.00 (m, 20 H, 4 C_6H_5) ppm. ^{31}P NMR (80.96 MHz, $CDCl_3$): δ = −4.08 (d, 1 P), −5.15 (d, $J_{P\text{-}P}$ = 21.1 Hz, 1 P) ppm. ^{13}C{^{1}H} NMR(100.6 MHz, $CDCl_3$): δ = 158.21 (2 C), 157.57 (2 C), 141.88 (4 C), 141.06 (2 C), 140.20 (2 C), 140.08 (4 C), 139.87 (2 C), 139.83 (2 C), 139.65 (2 C), 139.23 (8 C), 139.14 (4 C), 138.67 (2 C), 138.55 (2 C), 138.43 (2 C), 137.71 (2 C), 137.36 (2 C), 137.29 (4 C), 137.27 (4 C), 136.81 (2 C), 136.77 (2 C), 136.62 (2 C), 136.55 (2 C), 73.60 (2 C) (C_{60} resonance), 134.82, 129.21, 128.73, 127.02, 125.52, 125.21, 123.92, 123.28, 123.19 (4 C_6H_5P, resonance), 103.62 (−OCO−), 21.72 (CHO), 21.60 (CH_2), 17.15 (CH_3) ppm. IR (KBr disk): $\tilde{\nu}$ = 2002 (s), 1934 (s), 1870 (vs) (C≡O), ν_{C60} 1434 (m), 1181 (w), 578 (w), 523 (s) (C_{60}) cm^{-1}. MS (FAB): *m*/*z* = 1488 {[M$^+$], ^{186}W}. UV/Vis (THF): λ_{max} (log ε) = 254.0 (4.93), 291.0 (4.56), 338.5 (4.45), 432.0 (3.98), 604.0 (3.46) nm. $[\alpha]_{365}^{25}$ = −3.00 ($c = 2.02 \times 10^{-5}$ mol/L, THF). $C_{94}H_{32}O_5P_2W$ (1487.08): calcd. C 75.92, H 2.17; found C 75.64, H 2.45.

[(η²-C_{60})Pd{(−)-DIOP}] (5): A three-necked flask equipped with a magnetic stirrer bar, a rubber septum and a nitrogen inlet tube was charged with C_{60} (0.018 g, 0.025 mmol) and 8 mL of toluene. The mixture was stirred until the solids were dissolved. When [Pd(PPh$_3$)$_4$] (0.029 g, 0.025 mmol) was added, the solution turned dark green immediately. After (−)-DIOP (0.025 g, 0.050 mmol) was added, the solution was stirred for 10 min. 20 mL of hexane was then carefully layered on the reaction mixture. The flask was left to stand for 1 d without disturbing and tiny black needles precipitated. After the precipitate was filtered, washed with pentane and dried in vacuo, 0.030 g (91%) of **5**·$C_6H_5CH_3$ was obtained. M.p. > 300 °C (dec.). ^{1}H NMR (200 MHz, $CDCl_3$): δ = 1.38 (s, 6 H, 2CH_3), 2.34 (s, 3 H, PhCH_3), 2.58−2.76 (m, 2 H, 2OCH), 3.30−4.24 (m, 4 H, 2CH_2), 7.16−7.94 (m, 25 H, 5 C_6H_5) ppm. ^{31}P NMR (200 MHz, $CDCl_3$): δ = 9.28 (s, 2 P) ppm. IR (KBr disk): $\tilde{\nu}$ = 3061 (w), 3018 (w), 2983 (w), 2933 (w), 2910 (w), 2879 (w), 2860 (w), 1571 (w), 1480 (w), 1459 (w), 1433 (s), 1370 (m), 1252 (m), 1218 (m), 1183 (m), 1159(m), 1099 (m), 1055 (s), 978 (m), 885 (m), 832 (m), 749 (s, sh), 735 (s), 692 (s), 577 (m), 527 (s), 507 (s) cm^{-1}. UV/Vis (toluene): λ_{max} (log ε) = 288.5 (4.57), 294.5 (4.58), 334.5 (4.54), 447.0 (3.97) nm. $C_{98}H_{40}O_2P_2Pd$ (1417.76): calcd. C 83.02, H 2.84; found C 83.12, H 3.08.

[(η²-C_{60})Pt{(−)-DIOP}] (6): The synthesis was similar to that of **5**, except that [Pt(PPh$_3$)$_4$] (0.031 g, 0.025 mmol) was used instead of [Pd(PPh$_3$)]. 0.036 g (96%) of **6**·$C_6H_5CH_3$ as tiny black needles was obtained. M.p. > 300 °C (dec.). ^{1}H NMR (200 MHz, $CDCl_3$): δ = 1.37 (s, 6 H, 2 CH_3), 2.33 (s, 3 H, PhCH_3), 2.60−2.82 (m, 2 H, 2 OCH), 3.58−4.20 (m, 4 H, 2 CH_2), 7.10−8.04 (m, 25 H, 5 C_6H_5) ppm. ^{31}P NMR (200 MHz, $CDCl_3$): δ = 11.13 (s, $J_{Pt\text{-}P}$ = 3749 Hz, 2 P) ppm. IR (KBr disk): $\tilde{\nu}$ = 3057 (w), 3022 (w), 2983 (w), 2941 (w), 2910 (w), 2879 (w), 2860 (w), 1571 (w), 1478 (w), 1458 (w), 1434 (m), 1372 (w), 1332 (w), 1251 (m), 1218 (m), 1183 (m), 1160 (m), 1102 (m), 1057 (s), 979 (m), 884 (m), 832 (m), 784 (m), 745 (s, sh), 734 (s), 692 (s), 576 (m), 527 (s), 508 (s) cm^{-1}. UV/Vis (toluene): λ_{max} (log ε) = 288.5 (4.59), 295.0 (4.59), 334.5 (4.51), 438.5 (4.11) nm. $C_{98}H_{40}O_2P_2Pt$ (1506.42): calcd. C 78.14, H, 2.68. found C 78.40, H 2.67.

Crystal Structure Determination of 6: Single crystals of **6** suitable for X-ray diffraction analysis were obtained by slow diffusion of hexane into the toluene solution of **6** at ambient temperature. A crystal of **6** was glued to a glass fiber and mounted on a Bruker SMART-1000 automated diffractometer. Data were collected at room temperature, using graphite-monochromated Mo-K_α radiation (λ = 0.71073 Å) in the ω-2θ scanning mode. Absorption correction was performed using the SADABS method. The structure was solved by direct methods using the SHELXS-97 program[28] and refined by full-matrix least-squares techniques (SHELXL-97)[29] on F^2. Hydrogen atoms were located by using the geometric method. The crystal data and structural refinement details are listed in Table 6. The calculations were performed using the TEXSAN crystallographic software package of Molecular Structure Corporation. Crystallographic data (excluding structure factors) for the structure reported in this paper have been deposited with the Cambridge Crystallographic Data Centre as supplementary publication no. CCDC-199653. Copies of the data can be obtained free of charge on application to CCDC, 12 Union Road, Cambridge, CB2 1EZ, UK [Fax: (internat.) + 44-1223/336033; E-mail: deposit@ccdc.cam.ac.uk or www:http://www.ccdc.cam.ac.uk].

Table 6. Crystal data and structure refinements for $6{\cdot}C_6H_5CH_3$

Empirical formula	$C_{91}H_{32}O_2P_2Pt{\cdot}C_6H_5CH_3$
Formula mass	1506.33
Temperature [K]	293(2)
Crystal system	orthorhombic
Space group	$P2_12_12_1$
a [Å]	10.058(2)
b [Å]	24.389(5)
c [Å]	25.137(6)
V [Å^3]	6166(2)
Z	4
$d_{calcd.}$ [Mg·m^3]	1.623
μ [mm^{-1}]	2.390
$F(000)$	3008
Unique reflections, R_{int}	10 833, 0.0574
Observed reflections	7092
Goodness-of-fit on F^2	0.999
R [$I > 2\sigma(I)$]	$R_1 = 0.0453$
	$wR_2 = 0.1025$
R (all data)	$R_1 = 0.0821$
	$wR_2 = 0.1165$

Acknowledgments

We are grateful to the National Natural Science Foundation of China and the Laboratory of Organometallic Chemistry for financial support of this work. P. Z. gratefully acknowledges financial support from the University of Siena.

[1] For reviews, see for example: [1a] P. J. Fagan, J. C. Calabrese, B. Malone, *Acc. Chem. Res.* **1992**, *25*, 134−142. [1b] M. L. H. Green, *Pure Appl. Chem.* **1995**, *67*, 249−256. [1c] W. Sliwa, *Transition Met. Chem.* **1996**, *21*, 583−592. [1d] A. L. Balch, M. M. Olmstead, *Chem. Rev.* **1998**, *98*, 2123−2166. [1e] J. R. Bowser, *Adv. Organomet. Chem.* **1994**, *36*, 57−94.

[2] H. W. Kroto, J. R. Heath, S. C. O'Brien, R. F. Curl, R. E. Smalley, *Nature* **1985**, *318*, 162−163.

[3] W. Kräschmer, L. D. Lamb, K. Fostiropoulos, D. R. Huffman, *Nature* **1990**, *347*, 354−358.

[4] P. J. Fagan, J. C. Calabrese, B. Malone, *Science* **1991**, *252*, 1160−1161.

[5] For mononuclear [60]fullerene derivatives, see for example: [5a] A. L. Balch, V. J. Catalano, J. W. Lee, M. M. Olmstead, *J. Am. Chem. Soc.* **1992**, *114*, 5455−5457. [5b] V. V. Bashilov, P. V. Petrovskii, V. I. Sokolov, S. V. Lindeman, I. A. Guzey, Y. T. Struchkov, *Organometallics* **1993**, *12*, 991−992. [5c] H.-F. Hsu, Y. Du, T. E. Albrecht-Schmitt, S. R. Wilson, J. R. Shapley, *Organometallics* **1998**, *17*, 1756−1761.

[6] For dinuclear [60]fullerene derivatives, see for example: [6a] A. L. Balch, J. W. Lee, B. C. Noll, M. M. Olmstead, *J. Am. Chem. Soc.* **1992**, *114*, 10984−10985. [6b] S. Zhang, T. L. Brown, Y. Du, J. R. Shapley, *J. Am. Chem. Soc.* **1993**, *115*, 6705−6709. [6c] I. J. Mavunkal, Y. Chi, S.-M. Peng, G.-H. Lee, *Organometallics* **1995**, *14*, 4454−4456.

[7] For trinuclear [60]fullerene derivatives, see for example: [7a] H.-F. Hsu, J. R. Shapley, *J. Am. Chem. Soc.* **1996**, *118*, 9192−9193. [7b] J. T. Park, H. Song, J.-J. Cho, M.-K. Chung, J.-H. Lee, I.-H. Suh, *Organometallics* **1998**, *17*, 227−236.

[8] For multinuclear [60]fullerene derivatives, see for example: [8a] P. J. Fagan, J. C. Calabrese, B. Malone, *J. Am. Chem. Soc.* **1991**, *113*, 9408−9409. [8b] M. Rasinkangas, T. T. Pakkaned, T. A. Pakkaned, M. Ahlgrén, J. Rouvinen, *J. Am. Chem. Soc.* **1993**, *115*, 4901. [8c] K. Lee, Z.-H. Choi, Y.-J. Cho, H. Song, J. T. Park, *Organometallics* **2001**, *20*, 5564−5570.

[9] V. V. Bashilov, P. V. Petrovskii, V. I. Sokolov, *Russ. Chem. Bull.* **1993**, *42*, 392−393.

[10] V. V. Bashilov, P. V. Petrovskii, V. I. Sokolov, F. M. Dolgushin, A. I. Yanovsky, Yu. T. Struchkov, *Russ. Chem. Bull.* **1996**, *45*, 1207−1213.

[11] [11a] L.-C. Song, J.-T. Liu, Q.-M. Hu, G.-F. Wang, P. Zanello, M. Fontani, *Organometallics* **2000**, *19*, 5342−5351. [11b] L.-C. Song, Y.-H. Zhu, Q.-M. Hu, *J. Chem. Res. (S)* **2000**, 316−317. [11c] P. Zanello, F. Laschi, M. Fontani, L.-C. Song, Y.-H. Zhu, *J. Organomet. Chem.* **2000**, *593−594*, 7−11. [11d] Y.-H. Zhu, L.-C. Song, Q.-M. Hu, C.-M. Li, *Org. Lett.* **1999**, *1*, 1693−1695. [11e] L.-C. Song, Y.-H. Zhu, Q.-M. Hu, *Polyhedron* **1997**, *16*, 2141−2143. [11f] L.-C. Song, Y.-H. Zhu, Q.-M. Hu, *Polyhedron* **1998**, *17*, 469−473. [11g] Y.-L. Song, G.-Y. Fang, Y.-X. Wang, S. -T Liu, C.-F. Li, L.-C. Song, Y.- H. Zhu, Q.-M. Hu, *Appl. Phys. Lett.* **1999**, *74*, 332−334. [11h] L.-C. Song, Y.-H. Zhu, Q.-M. Hu, *J. Chem. Res. (S)* **1999**, 56−57. [11i] L.-C. Song, J.-T. Liu, Q.-M. Hu, L.-H. Weng, *Organometallics* **2000**, *19*, 1643−1647.

[12] U. Hengartner, D. Valentine, Jr., K. K. Johnson, M. E. Larscheid, F. Pigott, F. Scheidl, J. W. Scott, R. C. Sun, J. M. Townsend, T. Williams, *J. Org. Chem.* **1979**, *44*, 3741−3747.

[13] H. G. Horn, K. Sommer, *Spectrochim. Acta, Part A* **1971**, *27*, 1049−1054.

[14] M. L. H. Green, A. H. H. Stephens, *Chem. Commun.* **1997**, 793−794.

[15] R. E. Douthwaite, M. L. H. Green, A. H. H. Stephens, J. F. C. Turner, *J. Chem. Soc., Chem. Commun.* **1993**, 1522−1524.

[16] J. P. Hare, T. J. Dennis, H. W. Kroto, R. Taylor, A. W. Allaf, S. Balm, D. R. M. Walton, *J. Chem. Soc., Chem. Commun.* **1991**, 412−413.

[17] D. J. Darenbourg, D. J. Zalewski, C. Plepys, C. Campana, *Inorg. Chem.* **1987**, *26*, 3727−3732.

[18] J. P. Collman, L. S. Hegedus, J. R. Norton, R. J. Finke, *Principles and Applications of Organotransition Metal Chemistry*, 2nd ed., University Science Books, Mill Valley, CA, **1987**.

[19] [19a] R. Taylor, J. P. Hare, A. K. Abdul-Sada, H. W. Kroto, *J. Chem. Soc., Chem. Commun.* **1990**, 1423−1425. [19b] J. P. Hare, H. W. Kroto, R. Taylor, *Chem. Phys. Lett.* **1991**, *177*, 394−398. [19c] T. Akasaka, W. Ando, K. Kobagashi, S. Nagase, *J. Am. Chem. Soc.* **1993**, *115*, 1605−1606.

[20] A. N. Chernega, M. L. H. Green, J. Haggitt, A. H. H. Stephen, *Dalton Trans.* **1998**, 755−767.

[21] [21a] V. I. Sokolov, *Pure Appl. Chem.* **1998**, *70*, 789−798. [21b] V. I. Sokolov, *Russ. J. Org. Chem.* **1999**, *35*, 1257−1263. [21c] V. I. Sokolov, V. V. Bashilov, *Platinum Met.Rev.* **1998**, *42*, 18−24.

[22] P. Zanello, in *Chemistry at the Beginning of the Third Millennium* (Eds.: L. Fabbrizzi, A. Poggi), Springer, Heidelberg, **2000**, pp. 247−278.

[23] [23a] P. Zanello, F. Laschi, M. Fontani, C. Mealli, A. Ienco, K. Tang, X. Jin, L. Li, *J. Chem. Soc., Dalton Trans.* **1999**, 965−970. [23b] P. Zanello, F. Laschi, A. Cinquantini, M. Fontani, K. Tang, X. Jin, L. Li, *Eur. J. Inorg. Chem.* **2000**, 1345−1350.

[24] F. E. Mabbs, D. Collison, "Electron Paramagnetic Resonance of d Transition Metal Compounds", in *Studies in Inorganic Chemistry*, Elsevier, New York, **1992**, vol. 16.

[25] G. P. Lozos, C. G. Franz, *QCPE* **1991**, *23*, 20.

[26] L. Malatesta, M. Angoletta, *J. Chem. Soc.* **1957**, 1186−1188.

[27] L. Malatesta, C. Cariello, *J. Chem. Soc.* **1958**, 2323−2328.

[28] G. M. Sheldrick, *SHELXS-97, A Program for Crystal Structure Solution*, University of Göttingen, Germany, **1997**.

[29] G. M. Sheldrick, *SHELXL-97, A Program for Crystal Structure Refinement*, University of Göttingen, Germany, **1997**.

Received February 22, 2003

